

THE STANDARD MODEL AND THE TOP QUARK

Scott Willenbrock

Physics Department

University of Illinois at Urbana-Champaign

1110 W. Green St., Urbana, IL 61801

willen@uiuc.edu

Abstract

The top quark is one of the least well-studied components of the standard model. In these lectures I discuss the expected properties of the top quark, which will be tested at the Fermilab Tevatron and the CERN Large Hadron Collider. I begin with a modern review of the standard model, emphasizing the underlying concepts. I then discuss the role the top quark plays in precision electroweak analyses. The last two lectures address the strong and weak interactions of the top quark, with an emphasis on the top-quark spin.

The top quark is the least well-studied of the quarks. Why is the top quark an interesting and worthwhile object to study? Here are four of the most compelling reasons:

- A more accurate measurement of the top-quark mass is valuable as an input to precision electroweak analyses.
- We would like to know if the top quark is just an ordinary quark, or if it is exotic in some way.
- The top quark may be useful to discover new particles. For example, of all the fermions, the Higgs boson couples most strongly to the top quark. It might be possible to observe the Higgs boson produced in association with a $t\bar{t}$ pair.
- Events containing top quarks are backgrounds to new physics that we hope to discover. This may sound mundane, but it is extremely important. For example, the discovery of the top quark itself was only possible once we understood the background from $W+jets$.

Although these lectures are principally about the top quark, I have chosen to broaden them to include a review of the standard model. The top quark is very much a part of the standard model, and it is useful to discuss the physics of the top quark from that perspective. The physics of the top quark is a vast subject, and cannot be covered in a few lectures. Instead, I have chosen several subjects of broad interest related to the top quark, and discuss them in some depth, with an emphasis on the underlying concepts. I have also included several exercises with each lecture, which I strongly urge you to perform. They will engage you with the material in a way that will help solidify your understanding. The exercises can be performed using only material contained in these lectures. The exercises are of various levels of difficulty, indicated by * (easy), ** (moderate), and *** (hard). Solutions are provided in an appendix.

The first lecture is a review of the standard model from a modern point of view. It assumes the reader already has some familiarity with the standard model, and concentrates on the concepts that underlie the theory. The second lecture discusses the role the top quark plays in precision electroweak analyses via one-loop processes. The third and fourth lectures discuss the strong and weak interactions of the top quark, respectively, with an emphasis on the top-quark spin.

1. The Standard Model

In Table 1 I list the fermion fields that make up the standard model, along with their $SU(3) \times SU(2) \times U(1)_Y$ quantum numbers. The index $i = 1, 2, 3$ on each field refers to the generation, and the subscript L, R refers to the chirality of the field ($\psi_{L,R} \equiv \frac{1}{2}(1 \mp \gamma_5)\psi$). The left-chiral and right-chiral fields corresponding to a given particle have different $SU(2) \times U(1)$ quantum numbers, which leads to parity violation in the weak interaction.

Let's break the Lagrangian of the standard model into pieces. First consider the pure gauge interactions, given by

$$\mathcal{L}_{Gauge} = \frac{1}{2g_S^2} \text{Tr } G^{\mu\nu} G_{\mu\nu} + \frac{1}{2g^2} \text{Tr } W^{\mu\nu} W_{\mu\nu} - \frac{1}{4} B^{\mu\nu} B_{\mu\nu} , \quad (1)$$

where $G^{\mu\nu}$ is the field-strength tensor of the gluon field, $W^{\mu\nu}$ is that of the weak-boson field, and $B^{\mu\nu}$ is that of the hypercharge-boson field. These terms contain the kinetic energy of the gauge bosons and their self interactions. Next comes the gauge interactions of the fermion (“matter”) fields,

$$\mathcal{L}_{Matter} = i\bar{Q}_L^i \not{D} Q_L^i + i\bar{u}_R^i \not{D} u_R^i + i\bar{d}_R^i \not{D} d_R^i + i\bar{L}_L^i \not{D} L_L^i + i\bar{e}_R^i \not{D} e_R^i , \quad (2)$$

Table 1. The fermion fields of the standard model and their gauge quantum numbers.

				<u>$SU(3)$</u>	<u>$SU(2)$</u>	<u>$U(1)_Y$</u>
$Q_L^i =$	$\begin{pmatrix} u_L \\ d_L \end{pmatrix}$	$\begin{pmatrix} c_L \\ s_L \end{pmatrix}$	$\begin{pmatrix} t_L \\ b_L \end{pmatrix}$	3	2	$\frac{1}{6}$
$u_R^i =$	u_R	c_R	t_R	3	1	$\frac{2}{3}$
$d_R^i =$	d_R	s_R	b_R	3	1	$-\frac{1}{3}$
$L_L^i =$	$\begin{pmatrix} \nu_{eL} \\ e_L \end{pmatrix}$	$\begin{pmatrix} \nu_{\mu L} \\ \mu_L \end{pmatrix}$	$\begin{pmatrix} \nu_{\tau L} \\ \tau_L \end{pmatrix}$	1	2	$-\frac{1}{2}$
$e_R^i =$	e_R	μ_R	τ_R	1	1	-1

These terms contain the kinetic energy and gauge interactions of the fermions, which depend on the fermion quantum numbers. For example,

$$\not{D} Q_L = \gamma^\mu (\partial_\mu + ig_S G_\mu + ig W_\mu + i \frac{1}{6} g' B_\mu) Q_L \quad (3)$$

since the field Q_L participates in all three gauge interactions. A sum on the index i , which represents the generation, is implied in the Lagrangian.

We have constructed the simplest and most general Lagrangian, given the fermion fields and gauge symmetries.¹ The gauge symmetries forbid masses for any of the particles. In the case of the fermions, masses are forbidden by the fact that the left-chiral and right-chiral components of a given fermion field have different $SU(2) \times U(1)_Y$ quantum numbers. For example, a mass term for the up quark,

$$\mathcal{L} = -m \bar{u}_L u_R + h.c. , \quad (4)$$

is forbidden by the fact that u_L is part of the $SU(2)$ doublet Q_L , so such a term violates the $SU(2)$ gauge symmetry (it also violates $U(1)_Y$).

Although we only imposed the gauge symmetry on the Lagrangian, it turns out that it has a good deal of global symmetry as well, associated with the three generations. Because all fermions are massless thus far in our analysis, there is no difference between the three generations - they are physically indistinguishable. This manifests itself as a global flavor

¹I will give a precise definition to “simplest” later in this lecture. For now, it means the minimum number of fields and derivatives are used in each term in the Lagrangian.

symmetry of the matter Lagrangian, Eq. (2), which is invariant under the transformations

$$\begin{aligned}
Q_L^i &\rightarrow U_{Q_L}^{ij} Q_L^j \\
u_R^i &\rightarrow U_{u_R}^{ij} u_R^j \\
d_R^i &\rightarrow U_{d_R}^{ij} d_R^j \\
L_L^i &\rightarrow U_{L_L}^{ij} L_L^j \\
e_R^i &\rightarrow U_{e_R}^{ij} e_R^j,
\end{aligned} \tag{5}$$

where each U is an arbitrary 3×3 unitary matrix.

Exercise 1.1 () Show this.*

Since there are five independent $U(3)$ symmetries, the global flavor symmetry of the Lagrangian is $[U(3)]^5$.

The Lagrangian thus far contains only three parameters, the couplings of the three gauge interactions. Their approximate values (evaluated at M_Z) are

$$\begin{aligned}
g_S &\approx 1 \\
g &\approx \frac{2}{3} \\
g' &\approx \frac{2}{3\sqrt{3}}.
\end{aligned}$$

These couplings are all of order unity.

Electroweak symmetry breaking – The theory thus far is very simple and elegant, but it is incomplete - all particles are massless. We now turn to electroweak symmetry breaking, which is responsible for generating the masses of the gauge bosons and fermions.

In the standard model, electroweak symmetry breaking is achieved by introducing another field into the model, the Higgs field ϕ , with the quantum numbers shown in Table 2. The simplest and most general Lagrangian for the Higgs field, consistent with the gauge symmetry, is

$$\mathcal{L}_{Higgs} = (D^\mu \phi)^\dagger D_\mu \phi + \mu^2 \phi^\dagger \phi - \lambda (\phi^\dagger \phi)^2. \tag{6}$$

Table 2. The Higgs field and its gauge quantum numbers.

	<u>$SU(3)$</u>	<u>$SU(2)$</u>	<u>$U(1)_Y$</u>
$\phi = \begin{pmatrix} \phi^+ \\ \phi^0 \end{pmatrix}$	1	2	$\frac{1}{2}$

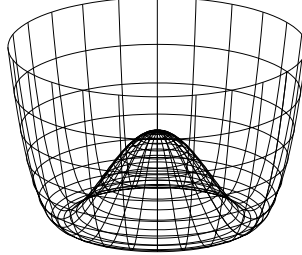


Figure 1. The Higgs potential. The neutral component of the Higgs field acquires a vacuum-expectation value $\langle\phi^0\rangle = v/\sqrt{2}$ on the circle of minima in Higgs-field space.

The first term contains the Higgs-field kinetic energy and gauge interactions. The remaining terms are (the negative of) the Higgs potential, shown in Fig. 1. The quadratic term in the potential has been chosen such that the minimum of the potential lies not at zero, but on a circle of minima

$$\langle\phi^0\rangle = \mu/\sqrt{2\lambda} \equiv \frac{v}{\sqrt{2}} \quad (7)$$

where ϕ^0 is the lower (neutral) component of the Higgs doublet field. This equation defines the parameter $v \approx 246$ GeV, the Higgs-field vacuum-expectation value. Making the substitution $\phi = (0, v/\sqrt{2})$ in the Higgs Lagrangian, Eq. (6), one finds that the W and Z bosons have acquired masses

$$M_W = \frac{1}{2}gv \quad M_Z = \frac{1}{2}\sqrt{g^2 + g'^2}v \quad (8)$$

from the interaction of the gauge bosons with the Higgs field. Since we know g and g' , these equations determine the numerical value of v .

The Higgs sector of the theory, Eq. (6), introduces just two new parameters, μ and λ . Rather than μ , we will use the parameter v introduced in Eq. (7). The parameter λ is the Higgs-field self interaction, and will not figure into our discussion.

Fermion masses and mixing – In quantum field theory, anything that is not forbidden is mandatory. With that in mind, there is one more set of interactions, involving the Higgs field and the fermions. The simplest and most general Lagrangian, consistent with the gauge symmetry, is

$$\mathcal{L}_{Yukawa} = -\Gamma_u^{ij}\bar{Q}_L^i\epsilon\phi^*u_R^j - \Gamma_d^{ij}\bar{Q}_L^i\phi d_R^j - \Gamma_e^{ij}\bar{L}_L^i\phi e_R^j + h.c. \quad (9)$$

where $\Gamma_u, \Gamma_d, \Gamma_e$ are 3×3 complex matrices in generation space.² We have therefore apparently introduced $3 \times 3 \times 3 \times 2 = 54$ new parameters into the theory, but as we shall see, only a subset of these parameters are physically relevant. These so-called Yukawa interactions of the Higgs field with fermions violate almost all of the $[U(3)]^5$ global symmetry of the fermion gauge interactions, Eq. (2). The only remaining global symmetries are the subset corresponding to baryon number

$$\begin{aligned} Q_L^i &\rightarrow e^{i\theta/3} Q_L^i \\ u_R^i &\rightarrow e^{i\theta/3} u_R^i \\ d_R^i &\rightarrow e^{i\theta/3} d_R^i \end{aligned} \quad (10)$$

and lepton number

$$\begin{aligned} L_L^i &\rightarrow e^{i\phi} L_L^i \\ e_R^i &\rightarrow e^{i\phi} e_R^i . \end{aligned} \quad (11)$$

Exercise 1.2 () Show this.*

The conservation of baryon number and lepton number follow from these symmetries. These symmetries are accidental; they are not put in by hand, but rather follow automatically from the field content and gauge symmetries of the theory. Thus we can say that we understand why baryon number and lepton number are conserved in the standard model.

Replacing the Higgs field with its vacuum-expectation value, $\phi = (0, v/\sqrt{2})$, in Eq. (9) yields

$$\mathcal{L}_M = -M_u^{ij} \bar{u}_L^i u_R^j - M_d^{ij} \bar{d}_L^i d_R^j - M_e^{ij} \bar{e}_L^i e_R^j + h.c. , \quad (12)$$

where

$$M^{ij} = \Gamma^{ij} \frac{v}{\sqrt{2}} \quad (13)$$

are fermion mass matrices. The Yukawa interactions are therefore responsible for providing the charged fermions with mass; the neutrinos, however, remain massless (we will discuss neutrino masses shortly).

The complete Lagrangian of the standard model is the sum of the gauge, matter, Higgs, and Yukawa interactions,

$$\mathcal{L}_{SM} = \mathcal{L}_{Gauge} + \mathcal{L}_{Matter} + \mathcal{L}_{Higgs} + \mathcal{L}_{Yukawa} . \quad (14)$$

²The matrix $\epsilon = \begin{pmatrix} 0 & 1 \\ -1 & 0 \end{pmatrix}$ in $SU(2)$ space is needed in order for the first term in Eq. (9) to respect $SU(2)$ gauge invariance.

This is the simplest and most general Lagrangian, given the field content and gauge symmetries of the standard model.

Given this Lagrangian, one can proceed to calculate any physical process of interest. However, it is convenient to first perform field redefinitions to make the physical content of the theory manifest. These field redefinitions do not change the predictions of the theory; they are analogous to a change of variables when performing an integration. To make the masses of the fermions manifest, we perform unitary field redefinitions on the fields in order to diagonalize the mass matrices in Eq. (12):

$$\begin{aligned} u_L^i &= A_{u_L}^{ij} u_L'^j & u_R^i &= A_{u_R}^{ij} u_R'^j \\ d_L^i &= A_{d_L}^{ij} d_L'^j & d_R^i &= A_{d_R}^{ij} d_R'^j \\ e_L^i &= A_{e_L}^{ij} e_L'^j & e_R^i &= A_{e_R}^{ij} e_R'^j \\ \nu_L^i &= A_{\nu_L}^{ij} \nu_L'^j \end{aligned} \quad (15)$$

Exercise 1.3 () Show that each matrix A must be unitary in order to preserve the form of the kinetic-energy terms in the matter Lagrangian, Eq. (2), e.g.*

$$\mathcal{L}_{KE} = i \bar{u}_L^i \not{\partial} u_L^i. \quad (16)$$

Once the mass matrices are diagonalized, the masses of the fermions are manifest. These transformations also diagonalize the Yukawa matrices Γ , since they are proportional to the mass matrices [see Eq. (13)]. However, we must consider what impact these field redefinitions have on the rest of the Lagrangian. They have no effect on the pure gauge or Higgs parts of the Lagrangian, Eqs. (1) and (6), which are independent of the fermion fields. They do impact the matter part of the Lagrangian, Eq. (2). However, a subset of these field redefinitions is the global $[U(3)]^5$ symmetry of the matter Lagrangian; this subset therefore has no impact.

One can count how many physically-relevant parameters remain after the field redefinitions are performed [1]. Let's concentrate on the quark sector. The number of parameters contained in the complex matrices Γ_u, Γ_d is $2 \times 3 \times 3 \times 2 = 36$. The unitary symmetries $U_{Q_L}, U_{u_R}, U_{d_R}$ are a subset of the quark field redefinitions; this subset will not affect the matter part of the Lagrangian. There are $3 \times 3 \times 3$ degrees of freedom in these symmetries (a unitary $N \times N$ matrix has N^2 free parameters), so the total number of parameters that remain in the full Lagrangian after field redefinitions is

$$2 \times 3 \times 3 \times 2 - (3 \times 3 \times 3 - 1) = 10 \quad (17)$$

where I have subtracted baryon number from the subset of field redefinitions that are symmetries of the matter Lagrangian. Baryon number

is a symmetry of the Yukawa Lagrangian, Eq. (9), and hence cannot be used to diagonalize the mass matrices.

Exercise 1.4 () Show that the quark field redefinitions are the symmetries $U_{Q_L}, U_{u_R}, U_{d_R}$ if $A_{u_L} = A_{d_L}$.*

The ten remaining parameters correspond to the six quark masses and the four parameters of the Cabibbo-Kobayashi-Maskawa (CKM) matrix (three mixing angles and one CP -violating phase). The CKM matrix is $V \equiv A_{d_L}^\dagger A_{u_L}$; we see that this matrix is unity if $A_{u_L} = A_{d_L}$, as expected from Exercise 1.4.

Exercise 1.5 () Show that V is unitary.*

The mass matrices are related to the Yukawa matrices by Eq. (13). If we make the natural assumption that the Yukawa matrices contain elements of order unity (like the gauge couplings), we expect the fermion masses to be of $\mathcal{O}(v)$, just like M_W and M_Z [see Eq. (8)]. This is not the case; only the top quark has such a large mass. We see that, from the point of view of the standard model, the question is not why the top quark is so heavy, but rather why the other fermions are so light.

Similarly, for a generic Yukawa matrix, one expects the field redefinitions that diagonalize the mass matrices to yield a CKM matrix with large mixing angles. Again, this is not the case; the measured angles are [2]

$$\begin{aligned}\theta_{12} &\approx 13^\circ \\ \theta_{23} &\approx 2.3^\circ \\ \theta_{13} &\approx 0.23^\circ \\ \delta &\approx 60^\circ\end{aligned}$$

which, with the exception of the CP -violating phase δ , are small.³ The question is not why these angles are nonzero, but rather why they are so small.

The fermion masses and mixing angles strongly suggest that there is a deeper structure underlying the Yukawa sector of the standard model. Surely there is some explanation of the peculiar pattern of fermion masses and mixing angles. Since the standard model can accommodate any masses and mixing angles, we must seek an explanation from physics beyond the standard model.

Beyond the Standard Model – Let us back up and ask: why did we stick to the simplest terms in the Lagrangian? The obsolete answer is

³The phase δ is the same as the angle γ of the so-called unitarity triangle.

that these are the renormalizable terms. Renormalizability is a stronger constraint than is really necessary. The modern answer, which is much simpler, is dimensional analysis [3].

We'll work with units such that $\hbar = c = 1$.

Exercise 1.6 () - Show that length has units of mass⁻¹, and hence $\partial_\mu = \partial/\partial x^\mu$ has units of mass.*

Since the action has units of $\hbar = 1$, the Lagrangian must have units of mass⁴, since

$$S = \int d^4x \mathcal{L} . \quad (18)$$

From the kinetic energy terms in the Lagrangian for a generic scalar (ϕ), fermion (ψ), and gauge boson (A^μ),

$$\mathcal{L}_{KE} = \partial^\mu \phi^* \partial_\mu \phi + i\bar{\psi} \not{\partial} \psi - \frac{1}{2}(\partial^\mu A^\nu \partial_\mu A_\nu + \partial^\mu A^\nu \partial_\nu A_\mu) \quad (19)$$

we can deduce the dimensionality of the various fields:

$$\begin{aligned} \dim \phi &= \text{mass} \\ \dim \psi &= \text{mass}^{3/2} \\ \dim A^\mu &= \text{mass} . \end{aligned}$$

All operators (products of fields) in the Lagrangian of the Standard Model are of dimension four, except the operator $\phi^\dagger \phi$ in the Higgs potential, which is of dimension two. The coefficient of this term, μ^2 , is the only dimensionful parameter in the standard model; it (or, equivalently, $v \equiv \mu/\sqrt{\lambda}$) sets the scale of all particle masses.

Imagine that the Lagrangian at the weak scale is an expansion in some large mass scale M ,

$$\mathcal{L} = \mathcal{L}_{SM} + \frac{1}{M} \dim 5 + \frac{1}{M^2} \dim 6 + \dots , \quad (20)$$

where $\dim n$ represents all operators of dimension n . By dimensional analysis, the coefficient of an operator of dimension n has dimension mass⁴⁻ⁿ, since the Lagrangian has dimension mass⁴. At energies much less than M , the dominant terms in this Lagrangian will be those of \mathcal{L}_{SM} ; the other terms are suppressed by an inverse power of M . This is the modern reason why we believe the “simplest” terms in the Lagrangian are the dominant ones.

The least suppressed terms in the Lagrangian beyond the standard model are of dimension five. We should therefore expect our first observation of physics beyond the standard model to come from these terms.

Given the field content and gauge symmetries of the standard model, there is only one such term:

$$\mathcal{L}_5 = \frac{c^{ij}}{M} L_L^{iT} \epsilon \phi C \phi^T \epsilon L_L^j + h.c. , \quad (21)$$

where c^{ij} is a dimensionless matrix in generation space.⁴

*Exercise 1.7 (**)* - Show that a similar term, with L_L replaced by Q_L , is forbidden by $SU(3) \times U(1)_Y$ gauge symmetry.

This dimension-five operator contains the Higgs-doublet field twice and the lepton-doublet field twice.

Exercise 1.8 ()* - Show that \mathcal{L}_5 violates lepton number.

Replacing the Higgs-doublet field with its vacuum-expectation value, $\phi = (0, v/\sqrt{2})$, yields

$$\mathcal{L}_5 = -\frac{c^{ij}}{2} \frac{v^2}{M} \nu_L^{iT} C \nu_L^j + h.c. . \quad (22)$$

This is a Majorana mass term for the neutrinos. The recent observation of neutrino oscillations, which requires nonzero neutrino mass, is indeed our first observation of physics beyond the standard model.

*Exercise 1.9 (***)* Show that the Maki-Nakagawa-Sakata (MNS) matrix (the analogue of the CKM matrix in the lepton sector) has 6 physically-relevant parameters. (Note: c^{ij} is a complex, symmetric matrix.)

The moral is that when we are searching for deviations from the standard model, what we are really doing is looking for the effects of higher-dimension operators. Although there is only one operator of dimension five, there are dozens of operators of dimension six, some of which are listed below [4]:

$$\begin{aligned} & \bar{L}^i \gamma^\mu L^j \bar{L}^k \gamma_\mu L^m \\ & \bar{L}^i \gamma^\mu L^j \bar{Q}^k \gamma_\mu Q^m \\ & i \bar{Q}^i \gamma_\mu D_\nu G^{\mu\nu} Q^j \\ & \text{Tr } G^{\mu\nu} G_{\nu\rho} G_\mu^\rho \\ & \phi^\dagger \phi \text{Tr } W^{\mu\nu} W_{\mu\nu} \\ & \phi^\dagger D_\mu \phi \bar{e}_R^i \gamma^\mu e_R^j . \end{aligned}$$

⁴The 2×2 matrix ϵ in $SU(2)$ space was introduced in an earlier footnote. The 4×4 matrix $C = \begin{pmatrix} -\epsilon & 0 \\ 0 & \epsilon \end{pmatrix}$ in Dirac space is needed for Lorentz invariance.

Thus far, none of the effects of any of these operators have been observed. The best we can do is set lower bounds on M (assuming some dimensionless coefficient). These lower bounds range from 1 TeV to 10^{16} GeV, depending on the operator. As we explore nature at higher energy and with higher accuracy, we hope to begin to see the effects of some of these dimension-six operators.

The mass scale M corresponds to the mass of a particle that is too heavy to observe directly. At energies greater than M , the expansion of Eq. (20) is no longer useful, as each successive term is larger than the previous. Instead, one must explicitly add the new field of mass M to the model. For example, if nature is supersymmetric at the weak scale, one must add the superpartners of the standard-model fields to the theory and include their interactions in the Lagrangian. If we raise the mass scale of the superpartners to be much greater than the weak scale, then we can no longer directly observe the superpartners, and we return to a description in terms of standard-model fields, with an expansion of the Lagrangian in inverse powers of the mass scale of the superpartners, M .

2. Virtual Top Quark

The top quark plays an important role in precision electroweak analyses. In this lecture I hope to clarify this sometimes confusing subject.

Recall from the previous lecture that the gauge, matter, and Higgs sectors of the standard model depend on only five parameters: the three gauge couplings, g_S , g , g' , and the Higgs-field vacuum-expectation value and self interaction, v and λ . At tree level, all electroweak quantities depend on just three of these parameters, g , g' , and v . We use the three best-measured electroweak quantities to determine these three parameters at tree level:

$$\begin{aligned}\alpha &= \frac{1}{4\pi} \frac{g^2 g'^2}{g^2 + g'^2} = \frac{1}{137.03599976(50)} \\ G_F &= \frac{1}{\sqrt{2}v^2} = 1.16637(1) \times 10^{-5} \text{ GeV}^{-2} \\ M_Z &= \frac{1}{2} \sqrt{g^2 + g'^2} v = 91.1876(21) \text{ GeV} ,\end{aligned}$$

where the uncertainty is given in parentheses. The value of α is extracted from low-energy experiments, G_F is extracted from the muon lifetime, and M_Z is measured from e^+e^- annihilation near the Z mass. From these three quantities, we can predict all other electroweak quantities at

tree level. For example, the W mass is

$$M_W^2 = \frac{1}{4}g^2v^2 = \frac{1}{2}M_Z^2 \left(1 + \sqrt{1 - \frac{4\pi\alpha}{\sqrt{2}G_F M_Z^2}} \right). \quad (23)$$

Exercise 2.1 () Verify the expression for M_W in terms of α , G_F , and M_Z .*

A more civilized expression for M_W is obtained by *defining*

$$s_W^2 \equiv 1 - \frac{M_W^2}{M_Z^2}. \quad (24)$$

This is the so-called “on-shell” definition⁵ of $\sin^2\theta_W$; it has a numerical value of $s_W^2 = 0.2228(4)$. Using this parameter, we can write a simpler expression than Eq. (23) for M_W at tree level:

$$M_W^2 = \frac{\frac{\pi\alpha}{\sqrt{2}G_F}}{s_W^2}. \quad (25)$$

Exercise 2.2 () - Verify this equation.*

At one loop this expression is modified:

$$M_W^2 = \frac{\frac{\pi\alpha}{\sqrt{2}G_F}}{s_W^2(1 - \Delta r)}, \quad (26)$$

where Δr contains the one-loop corrections. The top quark makes a contribution to Δr via the one-loop diagrams shown in Fig. 2, which contribute to the W and Z masses:

$$(\Delta r)_{\text{top}} \approx -\frac{3G_F m_t^2}{8\sqrt{2}\pi^2} \frac{1}{t_W^2}, \quad (27)$$

⁵So called because it is defined in terms of physical, or “on shell,” quantities.

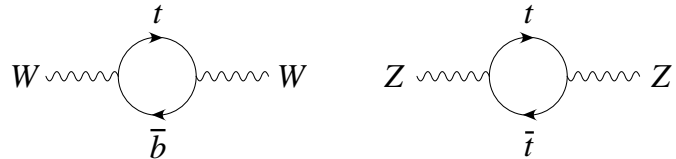


Figure 2. Virtual top-quark loops contribute to the W and Z masses.



Figure 3. Virtual Higgs-boson loops contribute to the W and Z masses.

where $t_W^2 \equiv \tan^2 \theta_W$. This one-loop correction depends quadratically on the top-quark mass.

The Higgs boson also contributes to Δr via the one-loop diagrams in Fig. 3:

$$(\Delta r)_{\text{Higgs}} \approx \frac{11G_F M_Z^2 c_W^2}{24\sqrt{2}\pi^2} \ln \frac{m_h^2}{M_Z^2}, \quad (28)$$

where $c_W^2 \equiv \cos^2 \theta_W$. This one-loop correction depends only logarithmically on the Higgs-boson mass, so Δr is not nearly as sensitive to m_h as it is to m_t .

Due to the contributions of the top quark and the Higgs boson to Δr , in order to predict M_W at one loop via Eq. (26) we need not just α , G_F , M_Z , but also m_t and m_h . Turning this around, in order to predict m_h , we need α , G_F , M_Z , and m_t , M_W . Thus a precision measurement of m_t and M_W can be used to predict the Higgs mass.

I show in Fig. 4 a plot of M_W vs. m_t , indicating lines of constant Higgs mass.⁶ The dashed ellipse indicates the 68% CL measurements of M_W and m_t ,

$$\begin{aligned} M_W &= 80.451(33) \text{ GeV} \\ m_t &= 174.3(5.1) \text{ GeV} \end{aligned}$$

(I will return to the solid ellipse momentarily). As you can see, the direct measurements of M_W and m_t favor a light Higgs boson.

*Exercise 2.3 (***)* - Derive the slope of the lines of constant Higgs mass on the plot of M_W vs. m_t . Evaluate it numerically and compare with the plot. [Hint: Derive dM_W^2/dm_t^2 and then evaluate $dM_W/dm_t = (m_t/M_W)dM_W^2/dm_t^2$ numerically. Be careful to use Eq. (24) for s_W^2 in Eq. (26) (you can neglect the dependence of t_W^2 on M_W in Eq. (27) since $(\Delta r)_{\text{top}}$ is a small correction).]

⁶The small arrow labeled $\Delta\alpha$ in that plot indicates the uncertainty in the lines of constant Higgs mass due to the uncertainty in $\alpha(M_Z)$.

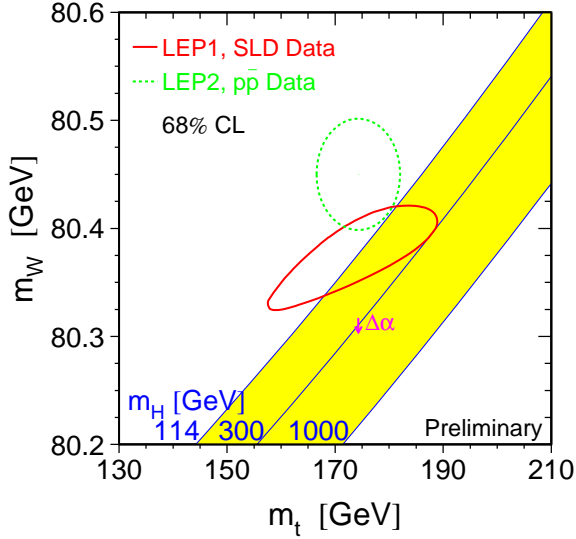


Figure 4. Lines of constant Higgs mass on a plot of M_W vs. m_t . The dashed ellipse is the 68% CL direct measurement of M_W and m_t . The solid ellipse is the 68% CL indirect measurement from precision electroweak data. From <http://lepewwg.web.cern.ch/LEPEWWG/>.

Neutral current – Rather than using the direct measurements of M_W and m_t to infer the Higgs-boson mass, one can use other electroweak quantities. The Fermi constant, G_F , is extracted from muon decay, which is a charged-current weak interaction. That leaves the neutral-current weak interaction as another quantity of interest. There is an enormous wealth of data on neutral-current weak interactions, such as e^+e^- annihilation near the Z mass, νN and eN deep-inelastic scattering, νe elastic scattering, atomic parity violation, and so on [2].

Let's consider a simple and very relevant example, the left-right asymmetry in e^+e^- annihilation near the Z mass, shown in Fig. 5. Left and right refer to the helicity of the incident electron, either negative (left) or positive (right). The asymmetry is defined in terms of the total cross section for a negative-helicity or positive-helicity electron to annihilate with an unpolarized positron and produce a Z boson,

$$A_{LR} \equiv \frac{\sigma_L - \sigma_R}{\sigma_L + \sigma_R}$$

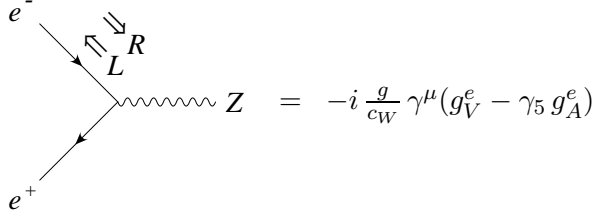


Figure 5. Neutral-current coupling of an electron to the Z boson. A left-handed electron has negative helicity, a right-handed electron has positive helicity.

$$= \frac{2g_V^e g_A^e}{g_V^{e2} + g_A^{e2}}, \quad (29)$$

where

$$\begin{aligned} g_V^e &= \sqrt{\rho_e} \left(-\frac{1}{2} + 2\kappa_e s_W^2 \right) \\ g_A^e &= \sqrt{\rho_e} \left(-\frac{1}{2} \right) \end{aligned} \quad (30)$$

are the vector and axial-vector couplings of the electron to the Z boson. At tree level, $\rho_e = \kappa_e = 1$, but there are one-loop corrections. The correction quadratic in the top-quark mass is

$$\begin{aligned} (\rho_e)_{\text{top}} &\approx 1 + \frac{3G_F m_t^2}{8\sqrt{2}\pi^2} \\ (\kappa_e)_{\text{top}} &\approx 1 + \frac{3G_F m_t^2}{8\sqrt{2}\pi^2} \frac{1}{t_W^2}. \end{aligned} \quad (31)$$

Different neutral-current measurements have different dependencies on m_t and m_h , so by combining two or more measurements one can extract both m_t and m_h . The solid ellipse in Fig. 4 represents the 68% CL constraint from all neutral-current measurements combined. It is in good agreement with the direct measurements of M_W and m_t , and strengthens the case for a light Higgs boson. Combining all precision electroweak data, one finds $45 \text{ GeV} \leq m_h \leq 191 \text{ GeV}$ [2].

Historically, neutral-current data were used to successfully predict the top-quark mass several years before it was discovered. This is a good reason to trust the prediction of a light Higgs boson from precision electroweak analyses.

It is also significant that the two ellipses in Fig. 4 lie on or near the lines of constant Higgs mass (within the allowed range of the Higgs mass). These measurements could have ended up far from those lines, thereby disproving the existence of the hypothetical Higgs boson. Instead, these measurements bolster our belief in the standard model in general, and in the Higgs boson in particular.

$\overline{\text{MS}}$ scheme – Before we leave this topic, let’s discuss the other most often-used definition of $\sin^2 \theta_W$. This is the minimal-subtraction-bar ($\overline{\text{MS}}$) scheme, so-called due to the simple way in which ultraviolet divergences in loop diagrams are subtracted.

Exercise 2.4 () - Show that*

$$\sin^2 \theta_W = \frac{g'^2}{g^2 + g'^2} \quad (32)$$

at tree level.

The $\overline{\text{MS}}$ scheme promotes this to the definition of $\sin^2 \theta_W$:

$$\hat{s}_Z^2 \equiv \frac{g'^2(M_Z)}{g^2(M_Z) + g'^2(M_Z)} \quad (33)$$

where the gauge couplings are evaluated at the Z mass. Its numerical value is $\hat{s}_Z^2 = 0.23113(15)$.

The analogues of Eqs. (26) and (24) in the $\overline{\text{MS}}$ scheme are

$$M_W^2 = \frac{\frac{\pi\alpha}{\sqrt{2}G_F}}{\hat{s}_Z^2(1 - \Delta\hat{r}_W)} \quad (34)$$

$$M_Z^2 = \frac{M_W^2}{\hat{c}_Z^2 \hat{\rho}}. \quad (35)$$

Unlike its on-shell analogue Δr , the one-loop quantity $\Delta\hat{r}_W$ has no quadratic dependence on the top-quark mass. This appears instead in the quantity $\hat{\rho}$ (which is unity in the on-shell scheme):

$$\hat{\rho} \approx 1 + \frac{3G_F m_t^2}{8\sqrt{2}\pi^2}. \quad (36)$$

Although the quadratic dependence on the top-quark mass has been shifted from one relation to another, the physical predictions, such as the constraint on the Higgs mass, remain unchanged.

*Exercise 2.5 (***) - Repeat Exercise 2.3 in the $\overline{\text{MS}}$ scheme. [Note that \hat{s}_Z^2 depends on M_W via Eq. (35).]*

3. Top Strong Interactions

We now begin to discuss the study of the top quark itself. In the introduction we listed several reasons why the top quark is an interesting object to study. The strategy that follows from these motivations is to get to know the top quark by measuring everything we can about it, and comparing with the predictions of the standard model. This program will occupy a large portion of our efforts at the Fermilab Tevatron and the CERN Large Hadron Collider (LHC). In this section I discuss some of the measurements that can be made at these machines related to the strong interactions of the top quark, and in the next section I turn to its weak interactions.

The top quark is produced at hadron colliders primarily via the strong interaction. The Feynman diagrams for the two contributing subprocesses, quark-antiquark annihilation and gluon fusion, are shown in Fig. 6. In Table 3 I give the predicted cross sections, at next-to-leading-order (NLO) in QCD, for $m_t = 175$ GeV. I also show the percentage of the cross section that results from each of the two subprocesses. At the Tevatron, the quark-antiquark-annihilation subprocess dominates; at the LHC, gluon fusion reigns. To understand why this is, we need to discuss the parton model of the proton.

The parton model is shown schematically in Fig. 7, where I illustrate how a proton-antiproton collision results in a $t\bar{t}$ pair produced via the

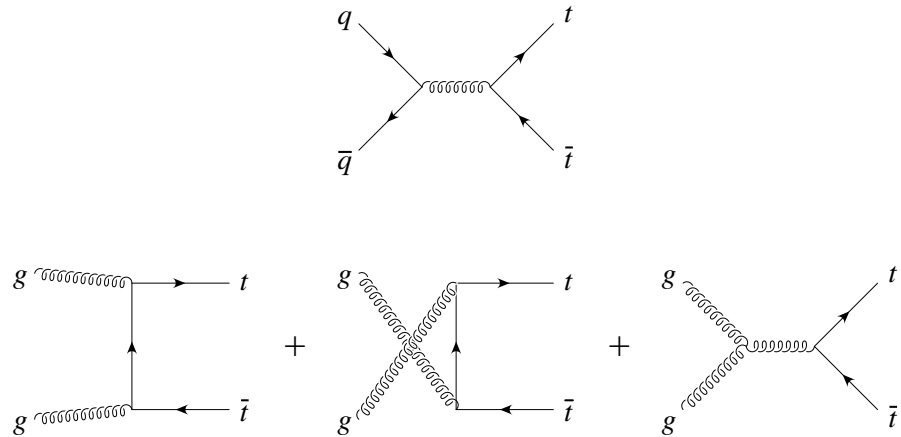


Figure 6. Top-quark production via the strong interaction at hadron colliders proceeds through quark-antiquark annihilation (upper diagram) and gluon fusion (lower diagrams).

Table 3. Cross sections, at next-to-leading-order in QCD, for top-quark production via the strong interaction at the Tevatron and the LHC [5]. Also shown is the percentage of the total cross section from the quark-antiquark-annihilation and gluon-fusion subprocesses.

	$\sigma_{\text{NLO}} (\text{pb})$	$q\bar{q} \rightarrow t\bar{t}$	$gg \rightarrow t\bar{t}$
Tevatron ($\sqrt{s} = 1.8 \text{ TeV } pp$)	$4.87 \pm 10\%$	90%	10%
Tevatron ($\sqrt{s} = 2.0 \text{ TeV } pp$)	$6.70 \pm 10\%$	85%	15%
LHC ($\sqrt{s} = 14 \text{ TeV } pp$)	$803 \pm 15\%$	10%	90%

quark-antiquark-annihilation subprocess. The proton is regarded as a collection of quarks, antiquarks, and gluons (collectively called partons), each carrying some fraction x of the proton's four-momentum. Figure 7 shows a proton of four-momentum P_1 colliding with an antiproton of four-momentum P_2 .

Exercise 3.1 () - Show that*

$$S \equiv (P_1 + P_2)^2 \approx 2P_1 \cdot P_2 \quad (37)$$

(neglecting the proton mass) is the square of the total energy in the center-of-momentum frame.

The quark is carrying fraction x_1 of the proton's four-momentum, the antiquark fraction x_2 of the antiproton's four-momentum. The square of the total energy of the partonic subprocess (in the partonic center-of-momentum frame) is similarly

$$\hat{s} \equiv (x_1 P_1 + x_2 P_2)^2 \approx 2x_1 x_2 P_1 \cdot P_2 = x_1 x_2 S. \quad (38)$$

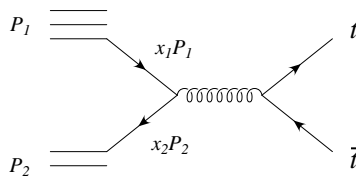


Figure 7. The parton-model description of top-quark pair production. A quark carrying fraction x_1 of the proton's momentum P_1 annihilates with an antiquark carrying fraction x_2 of the antiproton's momentum P_2 .

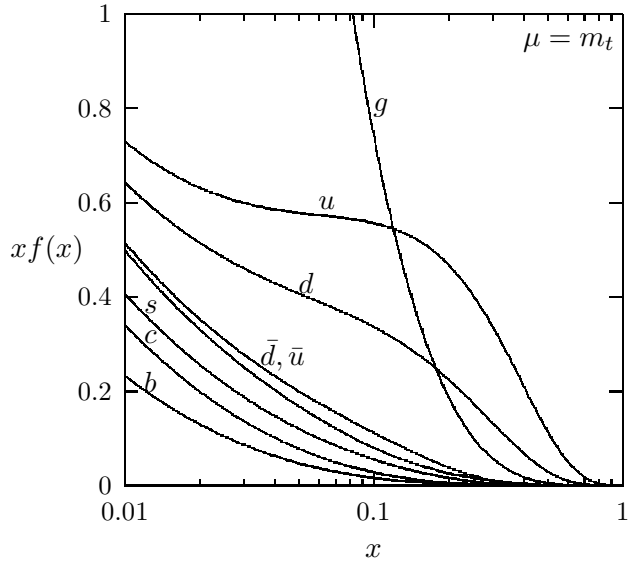


Figure 8. Parton distribution functions at the scale $\mu = m_t$, relevant for top-quark production.

Since there has to be at least enough energy to produce a $t\bar{t}$ pair at rest, $\hat{s} \geq 4m_t^2$. It follows from Eq. (38) that

$$x_1 x_2 = \frac{\hat{s}}{S} \geq \frac{4m_t^2}{S} . \quad (39)$$

Since the probability of finding a quark of momentum-fraction x in the proton falls off with increasing x , the typical value of $x_1 x_2$ is near the threshold for $t\bar{t}$ production. Setting $x_1 \approx x_2 = x$ in Eq. (39) gives

$$x \approx \frac{2m_t}{\sqrt{S}} \quad (40)$$

as the typical value of x for $t\bar{t}$ production.

Figure 8 shows the parton distribution functions in the proton for all the different species of partons.⁷ The probability of finding a given parton species with momentum fraction between x and $x+dx$ is $f(x)dx$. [What is plotted in Fig. 8 is actually $xf(x)$]. The parton distribution functions also depend on the relevant scale of the process, μ , which for top-quark production is of order m_t .

⁷I will explain in Section 4 the presence of antiquarks in the proton, as well as strange, charm, and bottom quarks.

The typical value of x for top-quark production may be computed from Eq. (40). For the typical value of x at the Tevatron, $x \approx 0.18$, the up distribution function is larger than that of the gluon, and the down distribution function is comparable to it. This explains why quark-antiquark annihilation dominates at the Tevatron. In contrast, for the typical value of x at the LHC, $x \approx 0.025$, the gluon distribution function is much larger than those of the quarks; this explains why gluon fusion reigns at the LHC.

Higgs and top – I mentioned in the introduction that the top quark could be used to discover the Higgs boson. To derive the coupling of the Higgs boson to fermions, write the Higgs-doublet field as

$$\phi = \begin{pmatrix} 0 \\ \frac{1}{\sqrt{2}}(v + h) \end{pmatrix} \quad (41)$$

where h is the Higgs boson, which corresponds to oscillations about the vacuum-expectation value of the field, Eq. (7). Inserting this expression for ϕ into the Yukawa Lagrangian, Eq. (9), yields the desired coupling, shown in Fig. 9.

*Exercise 3.2 (***)* - Show that the coupling of the Higgs boson to fermions is as given in Fig. 9. [Hint: Recall $M^{ij} = \Gamma^{ij}v/\sqrt{2}$, Eq. (13).]

The Feynman diagrams for Higgs-boson production in association with a $t\bar{t}$ pair are the same as those of Fig. 6, but with a Higgs boson attached to the top quark or antiquark. The Higgs boson can also be produced by itself via its coupling to a virtual top-quark loop, as shown in Fig. 10. Remarkably, this is the largest source of Higgs bosons at the Tevatron or the LHC. It is amusing that the virtual top quark points to the existence of a light Higgs boson, as discussed in the previous section, and may also help us discover the Higgs boson.

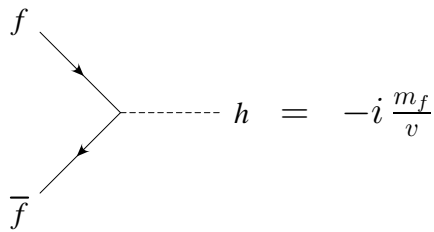


Figure 9. The coupling of the Higgs boson to fermions.

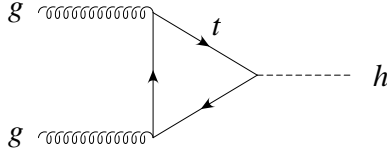


Figure 10. Higgs-boson production via gluon fusion through a top-quark loop.

Top-quark spin – One of the remarkable features of the top quark is that it is the only quark whose spin is directly observable. This is a consequence of its very short lifetime, $\Gamma_t^{-1} \approx (1.5 \text{ GeV})^{-1}$. Figure 11 shows an example of the evolution of a heavy quark of a definite spin after it is produced in a hard-scattering collision. On a time scale of order $\Lambda_{QCD}^{-1} \approx (200 \text{ MeV})^{-1}$, the heavy quark picks up a light antiquark of the opposite spin from the vacuum and hadronizes into a meson. Some time later, on the order of $(\Lambda_{QCD}^2/m_Q)^{-1} \approx (1 \text{ MeV})^{-1}$ (for $m_Q = m_t$), the spin-spin interaction between the heavy quark and the light quark⁸ cause the meson to evolve into a spin-zero state, $(|\uparrow\downarrow\rangle - |\downarrow\uparrow\rangle)/\sqrt{2}$, thereby depolarizing the heavy quark [6]. The top quark is the only quark that decays before it has a chance to depolarize (or even hadronize), so its spin is observable in the angular distribution of its decay products.⁹

Let's discuss the spin of a fermion in some detail. For a moving fermion, it is conventional to use the helicity basis, in which the spin quantization axis is the direction of motion of the fermion. The free

⁸This is the QCD analogue of the spin-spin interaction that produces the hyperfine splitting in atomic physics.

⁹Actually, the spin of a long-lived heavy quark is observable if it hadronizes into a baryon, such as a Λ_b .

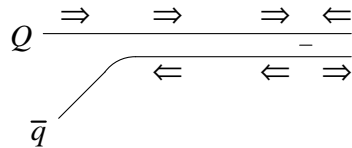


Figure 11. A heavy quark hadronizes with a light quark of the opposite spin, then evolves into a spin-zero meson.

fermion field may be decomposed into states of definite four-momentum,

$$\psi(x) = \int \frac{d^3p}{(2\pi)^3 \sqrt{2E}} \sum_{\lambda=\pm} (a_p^\lambda u_\lambda(p) e^{-ip \cdot x} + b_p^{\lambda\dagger} v_\lambda(p) e^{ip \cdot x}) , \quad (42)$$

where the sum is over positive and negative helicity, a_p^λ and $b_p^{\lambda\dagger}$ are the annihilation and creation operators for a fermion and an antifermion, and $u_\lambda(p)$ and $v_\lambda(p)$ are the momentum-space spinors for a fermion and an antifermion. These spinors are given explicitly in Table 4, in the representation where the Dirac matrices are [7]

$$\gamma^0 = \begin{pmatrix} 0 & 1 \\ 1 & 0 \end{pmatrix} \quad \gamma^i = \begin{pmatrix} 0 & \sigma^i \\ -\sigma^i & 0 \end{pmatrix} \quad \gamma_5 = \begin{pmatrix} -1 & 0 \\ 0 & 1 \end{pmatrix} , \quad (43)$$

where each entry in the above matrices is itself a 2×2 matrix.

We used the concept of chirality when formulating the standard model in Section 1. In the representation of the Dirac matrices given above,

$$\psi_L \equiv \frac{1 - \gamma_5}{2} \psi = \begin{pmatrix} 1 & 0 \\ 0 & 0 \end{pmatrix} \psi \quad (44)$$

$$\psi_R \equiv \frac{1 + \gamma_5}{2} \psi = \begin{pmatrix} 0 & 0 \\ 0 & 1 \end{pmatrix} \psi \quad (45)$$

so a left-chiral spinor has nonzero upper components and a right-chiral spinor has nonzero lower components. Chirality is conserved in gauge interactions because the matter Lagrangian, Eq. (2), connects fields of the same chirality. In the massless limit, helicity and chirality are related,

Table 4. Spinors for a fermion of energy E and three-momentum of magnitude p pointing in the (θ, ϕ) direction. The spinors $u_\lambda(p)$ and $v_\lambda(p)$ correspond to fermions and antifermions of helicity $\lambda(1/2)$.

$$u_+(p) = \begin{pmatrix} \sqrt{E-p} \begin{pmatrix} \cos \frac{\theta}{2} \\ e^{i\phi} \sin \frac{\theta}{2} \end{pmatrix} \\ \sqrt{E+p} \begin{pmatrix} \cos \frac{\theta}{2} \\ e^{i\phi} \sin \frac{\theta}{2} \end{pmatrix} \end{pmatrix} \quad u_-(p) = \begin{pmatrix} \sqrt{E+p} \begin{pmatrix} \sin \frac{\theta}{2} \\ -e^{i\phi} \cos \frac{\theta}{2} \end{pmatrix} \\ \sqrt{E-p} \begin{pmatrix} \sin \frac{\theta}{2} \\ -e^{i\phi} \cos \frac{\theta}{2} \end{pmatrix} \end{pmatrix}$$

$$v_+(p) = \begin{pmatrix} \sqrt{E+p} \begin{pmatrix} -e^{-i\phi} \sin \frac{\theta}{2} \\ \cos \frac{\theta}{2} \end{pmatrix} \\ -\sqrt{E-p} \begin{pmatrix} -e^{-i\phi} \sin \frac{\theta}{2} \\ \cos \frac{\theta}{2} \end{pmatrix} \end{pmatrix} \quad v_-(p) = \begin{pmatrix} \sqrt{E-p} \begin{pmatrix} e^{-i\phi} \cos \frac{\theta}{2} \\ \sin \frac{\theta}{2} \end{pmatrix} \\ -\sqrt{E+p} \begin{pmatrix} e^{-i\phi} \cos \frac{\theta}{2} \\ \sin \frac{\theta}{2} \end{pmatrix} \end{pmatrix}$$

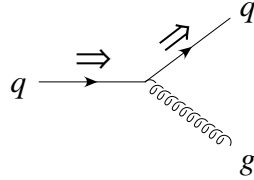


Figure 12. Helicity is conserved for massless quarks involved in a gauge interaction.

because the factor $\sqrt{E - p}$ vanishes in the expressions for the spinors in Table 4, causing either the upper or lower components to vanish:

$$\begin{aligned} u_+(p) &= u_R(p) & u_-(p) &= u_L(p) \\ v_+(p) &= v_L(p) & v_-(p) &= v_R(p) \end{aligned} \quad (46)$$

Note that the relationship between helicity and chirality is reversed for fermions and antifermions.

For massless fermions, chirality conservation implies helicity conservation, as shown in Fig. 12. For massive fermions, helicity is no longer related to chirality, so although chirality is conserved, helicity is not. This is illustrated in Fig. 13. Both helicity-conserving and helicity-nonconserving gauge interactions occur; the latter are proportional to the fermion mass, since they are forbidden in the massless limit.

Exercise 3.3 () - Do the quark mass terms in \mathcal{L}_M , Eq. (12), conserve chirality?*

A useful discrete symmetry of QCD is parity, $\mathbf{x} \rightarrow -\mathbf{x}$, $\mathbf{p} \rightarrow -\mathbf{p}$.

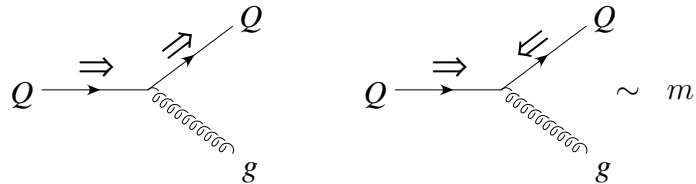


Figure 13. For massive quarks, there are helicity-conserving and nonconserving gauge interactions. The amplitude for the latter is proportional to the quark mass.

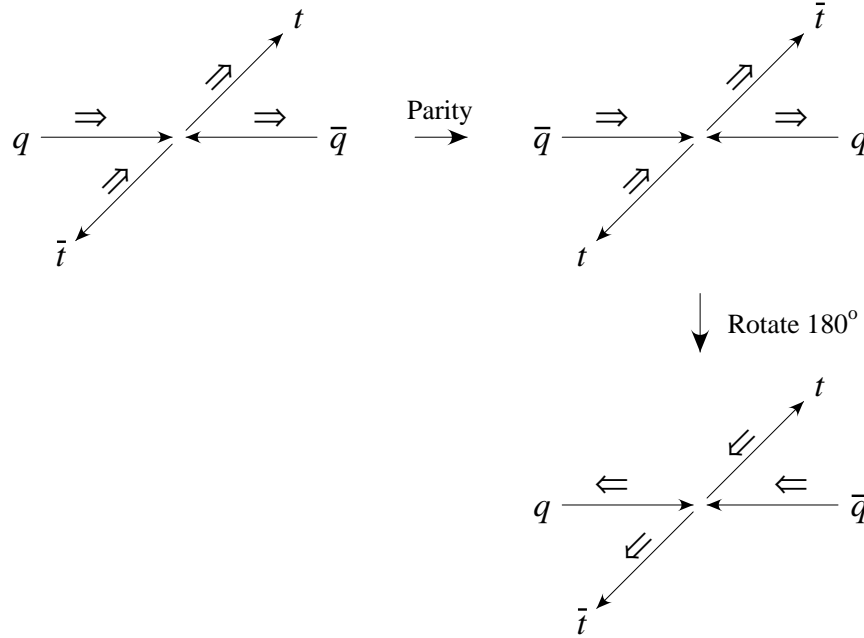


Figure 14. Parity and rotational symmetry are used to show that the top quark is produced unpolarized in (unpolarized) $p\bar{p}$ collisions.

Helicity flips under parity, because although spin does not flip,¹⁰ the direction of motion of the fermion does. One can show that the spinors of Table 4 are related to each other under parity as follows:

$$\begin{aligned} u_-(p) &= \gamma^0 u_+(\tilde{p}) \\ v_-(p) &= \gamma^0 v_+(\tilde{p}) \end{aligned} \quad (47)$$

where $p = (E, \mathbf{p})$, $\tilde{p} = (E, -\mathbf{p})$. This demonstrates that parity flips the helicity.

Parity can be used to show that top quarks are produced unpolarized in QCD reactions. Let's consider the quark-antiquark-annihilation subprocess, for example; a similar argument can be given for the gluon-fusion subprocess. In Fig. 14 I show a quark and an antiquark of opposite helicity annihilating to produce a top quark and a top antiquark of opposite helicity. (Due to helicity conservation in the massless limit, the

¹⁰Spin angular momentum, like orbital angular momentum ($\mathbf{L} = \mathbf{x} \times \mathbf{p}$), does not change sign under parity.

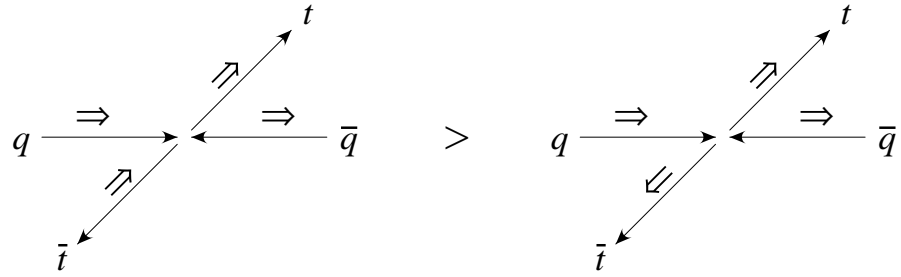


Figure 15. The cross section for opposite-helicity $t\bar{t}$ production is greater than that for same-helicity $t\bar{t}$ production.

helicities of the light quark and antiquark must be opposite; this is not true of the top quark and antiquark.) Applying a parity transformation to this reaction yields the second diagram in Fig. 14. Rotating this figure by 180° in the scattering plane yields the third diagram, which is the same as the first diagram but with all helicities reversed. Since parity is a symmetry of QCD, the rates for the first and third reactions are the same. The light quarks are unpolarized in (unpolarized) $p\bar{p}$ collisions, so the first and third reactions will occur with equal probabilities. The first reaction produces positive-helicity top quarks, the second negative-helicity top quarks. Thus top quarks are produced with positive and negative helicity with equal probability, *i.e.*, they are produced unpolarized.

However, there is another avenue open to observe the spin of the top quark. Although the top quark is produced unpolarized, the spin of the top quark is correlated with that of the top antiquark. This is shown in Fig. 15; the rate for opposite-helicity $t\bar{t}$ production is greater than that of same-helicity $t\bar{t}$ production.

Exercise 3.4 () - Argue that in the limit $E \gg m$, the correlation between the helicities of the top quark and antiquark is 100%.*

There is a special basis in which the correlation is 100% for all energies, dubbed the “off-diagonal” basis [8]. This basis is shown in Fig. 16. Rather than using the direction of motion of the quarks as the spin quantization axis, one uses another direction, which makes an angle ψ with respect to the beam, related to the scattering angle θ by

$$\tan \psi = \frac{\beta^2 \sin \theta \cos \theta}{1 - \beta^2 \sin^2 \theta}, \quad (48)$$

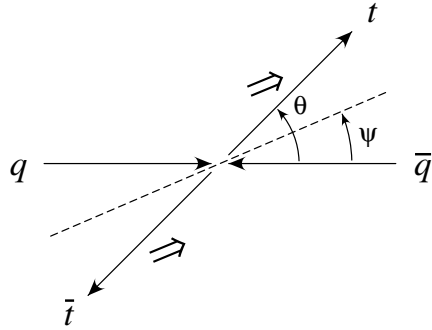


Figure 16. The “off-diagonal” basis. The spins of the top quark and antiquark point in the same direction.

where β is the velocity of the top quark and antiquark in the center-of-momentum frame. When the spin is projected along this axis, the correlation is 100%; the spins of the top quark and antiquark point in the same direction along this axis.

The moral of this story is that, for massive fermions, there is nothing special about the helicity basis. We will see this again in the next section on the weak interaction. The spin correlation between top quarks and antiquarks should be observed for the first time in Run II of the Tevatron.

Exercise 3.5 () - Use Eq. (48) to show that in the limit $E \gg m$, the off-diagonal basis is identical to the helicity basis. Argue that this had to be the case [Hint: See Exercise 3.4].*

*Exercise 3.6 (**) - What is the off-diagonal basis at threshold ($E = m$)? Give a physics argument for this basis at threshold.*

4. Top Weak Interactions

In this section I discuss the charged-current weak interaction of the top quark, shown in Fig. 17. This interaction connects the top quark with a down-type quark, with an amplitude proportional to the CKM matrix element V_{tq} ($q = d, s, b$). The interaction has a vector-minus-axial-vector ($V - A$) structure because only the left-chiral component of the top quark participates in the $SU(2)$ gauge interaction (see Table 1).

The charged-current weak interaction is responsible for the rapid decay of the top quark, as shown in Fig. 18. The partial width into the

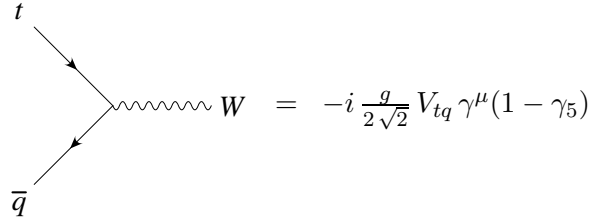


Figure 17. Charged-current weak interaction of the top quark.

final state Wq is proportional to $|V_{tq}|^2$.¹¹ The CDF Collaboration has measured [9]

$$\begin{aligned} \frac{BR(t \rightarrow Wb)}{BR(t \rightarrow Wq)} &= 0.94^{+0.31}_{-0.24} \\ &= \frac{|V_{tb}|^2}{|V_{td}|^2 + |V_{ts}|^2 + |V_{tb}|^2} \end{aligned} \quad (49)$$

This implies that $|V_{tb}| \gg |V_{td}|, |V_{ts}|$, but it does not tell us the absolute magnitude of V_{tb} .

Exercise 4.1 () - Show that the denominator of the last expression in Eq. (49) is unity if one assumes that there are just three generations.*

Thus, if we assume three generations, Eq. (49) implies $|V_{tb}| = 0.97^{+0.16}_{-0.12}$. However, we already know $V_{tb} = 0.9990 - 0.9993$ if there are just three generations [2].

¹¹The W boson then goes on to decay to a fermion-antifermion pair.

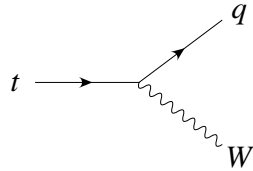


Figure 18. Top-quark decay via the charged-current weak interaction.

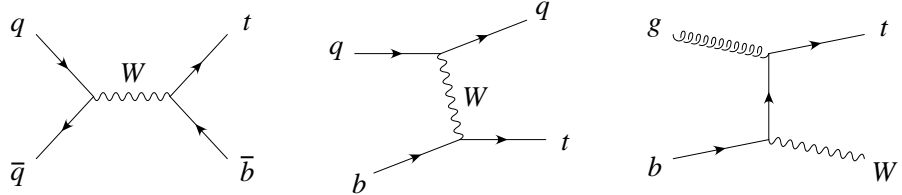


Figure 19. Single-top-quark production via the weak interaction. The first diagram corresponds to the s -channel subprocess, the second to the t -channel subprocess, and the third to Wt associated production (only one of the two contributing diagrams is shown).

Single top – The magnitude of V_{tb} can be extracted directly by measuring the cross section for top-quark production via the weak interaction. There are three such processes, depicted in Fig. 19, all of which result in a single top quark rather than a $t\bar{t}$ pair [10]. The cross sections for these single-top processes are proportional to $|V_{tb}|^2$.

The first subprocess in Fig. 19, which is mediated by the exchange of an s -channel W boson, is analogous to the Drell-Yan subprocess. The second subprocess is simply the first subprocess turned on its side, so the W boson is in the t channel. The b quark is now in the initial state, so this subprocess relies on the b distribution function in the proton, which we will discuss momentarily.¹² In the third subprocess, the W boson is real, and is produced in association with the top quark. This subprocess is also initiated by a b quark. The s - and t -channel subprocesses should be observed for the first time in Run II of the Tevatron; associated production of W and t must await the LHC.

The cross sections for these three single-top processes are given in Table 5 at the Tevatron and the LHC. The largest cross section at both ma-

¹²If one instead uses a d or s quark in the initial state, the cross section is much less due to the CKM suppression.

Table 5. Cross sections (pb), at next-to-leading-order in QCD, for top-quark production via the weak interaction at the Tevatron and the LHC [11, 12, 13].

	s channel	t channel	Wt
Tevatron ($\sqrt{s} = 2.0$ TeV $p\bar{p}$)	$0.90 \pm 5\%$	$2.1 \pm 5\%$	$0.1 \pm 10\%$
LHC ($\sqrt{s} = 14$ TeV pp)	$10.6 \pm 5\%$	$250 \pm 5\%$	$75 \pm 10\%$

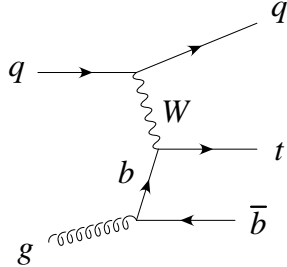


Figure 20. When the \bar{b} is produced at high transverse momentum, the leading-order process for t -channel single-top production is W -gluon fusion.

chines is from the t -channel subprocess; it is nearly one third of the cross section for $t\bar{t}$ pair production via the strong interaction (see Table 3). The next largest cross section at the Tevatron is from the s -channel subprocess. This is the smallest of the three at the LHC, because it is initiated by a quark-antiquark collision. As is evident from Fig. 8, the light-quark distribution functions grow with decreasing x more slowly than the gluon or b distribution functions, so quark-antiquark annihilation is relatively suppressed at the LHC. For a similar reason, associated production of W and t (which is initiated by a gluon- b collision) is relatively large at the LHC, while it is very small at the Tevatron.

Let's consider the largest of the three processes, t -channel single-top production, in more detail. This process was originally dubbed W -gluon fusion [14], because it was thought of as a virtual W striking a gluon to produce a $t\bar{b}$ pair, as shown in Fig. 20. If the \bar{b} in the final state is at high transverse momentum (p_T), this is indeed the leading-order diagram for this process. If we instead integrate over the p_T of the \bar{b} , we obtain an enhancement from the region where the \bar{b} is at low p_T , nearly collinear with the incident gluon.

*Exercise 4.2 (**)* - Show that a massless quark propagator blows up in the collinear limit, as shown in Fig. 21.

The b mass regulates the collinear divergence, such that the resulting cross section is proportional to $\alpha_S \ln(m_t^2/m_b^2)$, where the weak couplings are tacit.

This collinear enhancement is desirable — it yields a larger cross section — but it also makes perturbation theory less convergent. Each emission of a collinear gluon off the internal b quark produces another power of $\alpha_S \ln(m_t^2/m_b^2)$, because it yields another b propagator that is

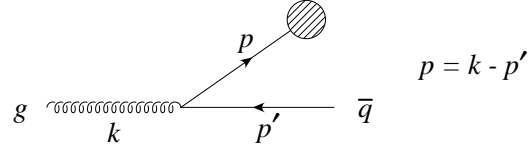


Figure 21. When a gluon splits into a real antiquark and a virtual quark, the quark propagator becomes singular when the kinematics are collinear.

nearly on-shell, as shown in Fig. 22. The result is that the expansion parameter for perturbation theory is $\alpha_S \ln(m_t^2/m_b^2)$, rather than α_S [12].

Fortunately, there is a simple solution to this problem. The collinear logarithms that arise are exactly the ones that are summed to all orders by the Dokshitzer-Gribov-Lipatov-Altarelli-Parisi (DGLAP) equations. In order to sum these logarithms, one introduces a b distribution function in the proton. When one calculates t -channel single-top production using a b distribution function, as in the second diagram in Fig. 19, one is automatically summing these logarithms to all orders. The expansion parameter for perturbation theory is now simply α_S [15].

Figure 23 shows how the b distribution function in the proton arises from a gluon splitting into a (virtual) $b\bar{b}$ pair. The strange and charm distributions arise in the same way; this also explains the presence of up and down antiquarks in the proton (see Fig. 8). Unlike the other “sea” quark distributions, which are extracted from experiment, the b distribution function is calculated from the initial condition $b(x) = 0$ at $\mu = m_b$, and is evolved to higher μ via the DGLAP equations.

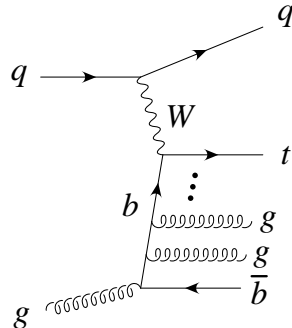


Figure 22. The emission of collinear gluons is suppressed only by $\alpha_S \ln(m_t^2/m_b^2)$, rather than α_S .

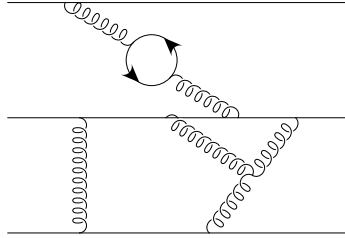


Figure 23. The quark “sea” in the proton arises from loops of virtual quarks.

*Exercise 4.3 (**)* - Draw the leading-order Feynman diagrams for the subprocesses that contribute to

- (a) $p\bar{p} \rightarrow W + X$
- (b) $p\bar{p} \rightarrow W + 1 \text{ jet} + X$

where X denotes the remnants of the proton and antiproton.

Top-quark spin – In the previous section we studied the top-quark spin in the context of the strong interaction. Let’s now consider this topic in relation to the weak interaction, beginning with the decay of the top quark.

The top-quark decay to the final state $b\bar{\ell}\nu$ is depicted in Fig. 24.

*Exercise 4.4 (**)* Determine the helicities of all final-state particles in top decay (neglecting their masses).

The partial width for this decay, summed over the two spin states of the top quark, is given by a very simple formula:

$$d\Gamma \sim \sum_{\text{spin}} |\mathcal{M}|^2 \sim t \cdot \ell b \cdot \nu, \quad (50)$$

where the four-momentum of the fermion or antifermion is denoted by its label. To undo the sum over the top-quark spin, it is useful to decompose

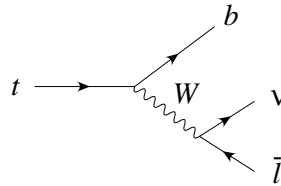


Figure 24. Semileptonic top-quark decay.

the four-momentum of the top quark, t , into two lightlike four vectors,

$$t = t_1 + t_2 \quad (51)$$

$$t_1 = \frac{1}{2}(t + ms) \quad (52)$$

$$t_2 = \frac{1}{2}(t - ms) \quad (53)$$

where s is the spin four-vector. In the top-quark rest frame, the spin four-vector is $s = (0, \hat{s})$, where \hat{s} is a unit vector that defines the spin quantization axis of the top quark.

Exercise 4.5 () - Show that t_1 and t_2 are lightlike four-vectors, $t_1^2 = t_2^2 = 0$.*

In the top-quark rest frame, the spatial components of t_1 point in the spin-up direction, while the spatial components of t_2 point in the spin-down direction. The partial widths for the decay of these two spin states are

$$\begin{aligned} d\Gamma_{\uparrow} &\sim t_2 \cdot \ell b \cdot \nu \\ d\Gamma_{\downarrow} &\sim t_1 \cdot \ell b \cdot \nu . \end{aligned} \quad (54)$$

Note that Eq. (50) is the sum of these two partial widths, as expected.

Let's consider the decay of a top quark with spin up along the \hat{s} direction in its rest frame, as depicted in Fig. 25. In this frame, the spatial components of t_2 point in the $-\hat{s}$ direction. Hence

$$d\Gamma_{\uparrow} \sim t_2 \cdot \ell \sim 1 + \cos \theta , \quad (55)$$

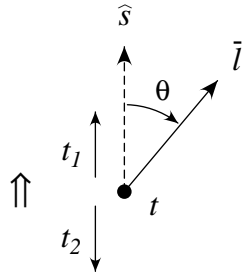


Figure 25. Semileptonic top-quark decay in the top rest frame. The vector \hat{s} indicates the spin-quantization axis. The four-vectors t_1 and t_2 have spatial components that point in the spin up and down directions, respectively.

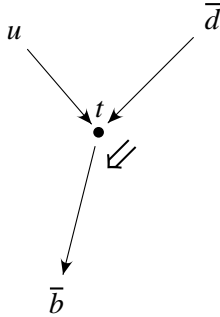


Figure 26. In single-top production, the top-quark spin is polarized along the direction of the \bar{d} quark in the top rest frame.

where θ is the angle between the spin direction and the charged-lepton three-momentum (see Fig. 25).

Exercise 4.6 () - Confirm Eq. (55).*

Thus

$$\frac{d\Gamma_{\uparrow}}{d\cos\theta} \sim 1 + \cos\theta, \quad (56)$$

which means that the charged lepton in top decay tends to go in the direction of the top-quark spin. In fact, the charged lepton is the most efficient analyzer of the top-quark spin, via the angular distribution of Eq. (56) [16].

We can use these same formulas to analyze the top-quark spin in single-top production [17]. The Feynman diagram for the s -channel subprocess, Fig. 19, is the same as that for top-quark decay, Fig. 24, with the replacement $\nu \rightarrow u$, $\ell \rightarrow \bar{d}$. Thus

$$\begin{aligned} d\sigma_{\uparrow} &\sim t_2 \cdot db \cdot u \\ d\sigma_{\downarrow} &\sim t_1 \cdot db \cdot u \end{aligned} \quad (57)$$

from Eqs. (54). If we choose the spin-quantization axis to point in the direction of the \bar{d} (in the top-quark rest frame), then $t_1 \sim d$, and the latter cross section above vanishes. Thus the top-quark is 100% polarized in the direction of the \bar{d} (in the top-quark rest frame) in s -channel single-top production, as depicted in Fig. 26. This result holds true for t -channel single-top production as well, since it proceeds via the same Feynman diagram, just turned on its side.

Although the top quark is 100% polarized when produced via the weak interaction, it is not in a state of definite helicity. Just as we saw

in the previous section, there is nothing special about helicity for massive fermions. It may be possible to observe the polarization of single top quarks in Run II of the Tevatron.

*Exercise 4.7 (***)* - Show that in the limit $E \gg m$, the top quark has negative helicity when produced via the s - or t -channel subprocesses, as expected.

Acknowledgments

I would like to thank Harrison Prosper for organizing a very memorable summer school. I am also grateful to Reinhard Schwienhorst and Martin Hennecke for reading the manuscript, and to Kevin Paul for preparing the figures. This work was supported in part by the U. S. Department of Energy under contract No. DOE DE-FG02-91ER40677.

Solutions to the exercises

Section 1

Exercise 1.1 – It is easiest to show this using index-free notation. Write the first term in the Lagrangian of Eq. (2) as

$$i\bar{Q}_L^i \not{D} Q_L^i = iQ_L^\dagger \gamma^0 \not{D} Q_L , \quad (58)$$

where Q_L is a 3-component vector in generation space. This term is invariant under the transformation $Q_L \rightarrow U_{Q_L} Q_L$, because the 3×3 unitary matrix U_{Q_L} commutes with the Dirac matrices (which are the same for all three generations):

$$iQ_L^\dagger \gamma^0 \not{D} Q_L \rightarrow iQ_L^\dagger U_{Q_L}^\dagger \gamma^0 \not{D} U_{Q_L} Q_L = iQ_L^\dagger \gamma^0 \not{D} Q_L , \quad (59)$$

where I have used $U_{Q_L}^\dagger U_{Q_L} = 1$. The same argument applies to the other fermionic terms in the Lagrangian and their corresponding symmetries.

Exercise 1.2 – Consider the transformation of the first term in the Yukawa Lagrangian, Eq. (9), under the symmetry U_{Q_L} of Eq. (5):

$$\bar{Q}_L^i \epsilon \phi^* u_R^j \rightarrow \bar{Q}_L^i U_{Q_L}^\dagger \epsilon \phi^* u_R^j . \quad (60)$$

This is not invariant under the symmetry transformation, so U_{Q_L} is violated. In contrast, baryon number symmetry, Eq. (10), is respected:

$$\bar{Q}_L^i \epsilon \phi^* u_R^j \rightarrow \bar{Q}_L^i e^{-i\theta/3} \epsilon \phi^* e^{i\theta/3} u_R^j = \bar{Q}_L^i \epsilon \phi^* u_R^j . \quad (61)$$

The same applies to the other terms in the Yukawa Lagrangian, and also to lepton number, Eq. (11).

Exercise 1.3 – Consider the transformation of the Lagrangian of Eq. (16) under the first field redefinition of Eq. (15) (using the index-free notation introduced in the solution to Exercise 1.1):

$$\mathcal{L}_{KE} = i\bar{u}_L \partial u_L \rightarrow i\bar{u}_L A_{u_L}^\dagger \partial A_{u_L} u_L = i\bar{u}_L \partial u_L . \quad (62)$$

The last step requires that A_{u_L} be unitary, $A_{u_L}^\dagger A_{u_L} = 1$. The same argument applies to the other fermionic kinetic-energy terms in the Lagrangian.

Exercise 1.4 – If $A_{u_L} = A_{d_L}$, then we may combine the first two field redefinitions in Eq. (15) into one equation:

$$Q_L^i = A_{Q_L}^{ij} u_L^j , \quad (63)$$

where $A_{Q_L} = A_{u_L} = A_{d_L}$. This is exactly the symmetry U_{Q_L} of Eq. (5). The field redefinitions of u_R^i and d_R^i in Eq. (15) are the symmetries U_{u_R} and U_{d_R} of Eq. (5).

Exercise 1.5 – This follows from the definition of the CKM matrix, $V \equiv A_{d_L}^\dagger A_{u_L}$:

$$V^\dagger V = (A_{d_L}^\dagger A_{u_L})^\dagger A_{d_L}^\dagger A_{u_L} = A_{u_L}^\dagger A_{d_L} A_{d_L}^\dagger A_{u_L} = 1 , \quad (64)$$

where I have used the unitarity of the A matrices.

Exercise 1.6 – A useful equation to remember is $\hbar c = 197$ MeV fm. Using this, one can convert length to mass $^{-1}$:

$$\text{length} = \hbar c / \text{mass } c^2 = \text{mass}^{-1} \quad (65)$$

using $\hbar = c = 1$.

Exercise 1.7 – Such a term is not invariant under SU(3) gauge symmetry, $Q_L \rightarrow U Q_L$, where U acts on the (suppressed) color indices of the quarks:

$$Q_L^{iT} \epsilon \phi C \phi^T \epsilon Q_L^j \rightarrow Q_L^{iT} U^T \epsilon \phi C \phi^T \epsilon U Q_L^j . \quad (66)$$

This involves $U^T U$, which is not equal to unity (rather, $U^\dagger U = 1$). This term is also not invariant under $U(1)_Y$, as the total hypercharge is nonzero $(1/6+1/6+1/2+1/2)$.

Exercise 1.8 – Lepton number, Eq. (11), is violated because

$$L_L^{iT} \epsilon \phi C \phi^T \epsilon L_L^j \rightarrow L_L^{iT} e^{i\phi} \epsilon \phi C \phi^T \epsilon e^{i\phi} L_L^j \quad (67)$$

is not invariant. Recall that lepton number is an accidental symmetry of the standard model. Once you go beyond the standard model by including higher-dimension operators, there is no reason for lepton number

(and baryon number) to be conserved.

Exercise 1.9 – We'll follow a similar argument to the one made to count the number of parameters in the CKM matrix. The Yukawa matrix Γ_e has $2 \times 3 \times 3$ parameters, and the complex, symmetric matrix c^{ij} has 2×6 parameters. The symmetries U_{L_L} and U_{e_R} contain $2 \times 3 \times 3$ degrees of freedom, so the number of physically-relevant parameters is

$$2 \times 3 \times 3 + 2 \times 6 - 2 \times 3 \times 3 = 12 . \quad (68)$$

[Note that we did not remove lepton number from the symmetries, because lepton number is violated by \mathcal{L}_5 , Eq. (21)]. Of these parameters, six are the charged-lepton and neutrino masses, leaving six parameters for the MNS matrix. Three are mixing angles, and three are CP -violating phases.

Section 2

Exercise 2.1 – Plug the expressions for α , G_F , and M_Z in terms of g , g' , and v , given at beginning of Section 2, into Eq. (23) and carry through the algebra to obtain $M_W^2 = (1/4)g^2v^2$.

Exercise 2.2 – Using Eq. (24), we can write Eq. (25) as

$$M_W^2 \left(1 - \frac{M_W^2}{M_Z^2} \right) = \frac{\pi\alpha}{\sqrt{2}G_F} . \quad (69)$$

Solving this quadratic equation for M_W^2 yields Eq. (23). Alternatively, one could plug the expressions for α , G_F , and M_Z in terms of g , g' , and v , given at beginning of Section 2, as well as $M_W^2 = (1/4)g^2v^2$, into the above equation to check its veracity.

Exercise 2.3 – Starting from Eq. (26), the one-loop analogue of Eq. (69) is

$$M_W^2 \left(1 - \frac{M_W^2}{M_Z^2} \right) = \frac{\frac{\pi\alpha}{\sqrt{2}G_F}}{(1 - \Delta r)} . \quad (70)$$

The differential of this equation (with respect to M_W^2 and m_t^2 , keeping everything else fixed) is

$$dM_W^2 - 2 \frac{M_W^2}{M_Z^2} dM_W^2 = - \frac{\frac{\pi\alpha}{\sqrt{2}G_F}}{(1 - \Delta r)^2} \frac{3G_F dm_t^2}{8\sqrt{2}\pi^2} \frac{1}{t_W^2} , \quad (71)$$

where I have used Eq. (27) for Δr . We can now set $\Delta r = 0$ to leading-order accuracy, and solve for dM_W^2/dm_t^2 :

$$\frac{dM_W^2}{dm_t^2} = \frac{3\alpha}{16\pi} \frac{1}{(2c_W^2 - 1)t_W^2} , \quad (72)$$

where I've used Eq. (24). Using $dM_W/dm_t = (m_t/M_W)dM_W^2/dm_t^2$ and evaluating numerically (for $M_W = 80$ GeV, $m_t = 175$ GeV) gives a slope of 0.0060, in good agreement with the slope of the lines of constant Higgs mass in Fig. 4.

Exercise 2.4 – The desired result follow from inserting $M_W^2 = (1/4)g^2v^2$ and $M_Z^2 = (1/4)(g^2 + g'^2)v^2$ [Eq. (8)] into the on-shell definition of $\sin^2 \theta_W$, Eq. (24).

Exercise 2.5 – Combining Eqs. (34) and (35) to eliminate \hat{s}_Z^2 gives

$$M_W^2 \left(1 - \frac{M_W^2}{M_Z^2 \hat{\rho}} \right) = \frac{\frac{\pi \alpha}{\sqrt{2} G_F}}{(1 - \Delta \hat{r}_W)}. \quad (73)$$

The differential of this equation is

$$dM_W^2 - 2 \frac{M_W^2}{M_Z^2 \hat{\rho}} dM_W^2 + \frac{M_W^4}{M_Z^2 \hat{\rho}^2} \frac{3G_F dm_t^2}{8\sqrt{2}\pi^2} = 0, \quad (74)$$

where I have used Eq. (35) for $\hat{\rho}$ (there is no m_t dependence in $\Delta \hat{r}_W$). We can now set $\hat{\rho} = 1$ to leading-order accuracy. Using the leading-order expressions of Eq. (25) and $M_W^2/M_Z^2 = c_W^2$, it is easy to show that Eq. (74) is identical Eq. (71) at leading order.

Section 3

Exercise 3.1 – The four-momenta of the quark and antiquark in the center-of-momentum frame are

$$\begin{aligned} P_1 &= (E, 0, 0, p) \\ P_2 &= (E, 0, 0, -p). \end{aligned}$$

Thus $S \equiv (P_1 + P_2)^2 = (2E, 0, 0, 0)^2 = (2E)^2$, which is the square of the total energy of the collision. The last expression in Eq. (37) follows from $(P_1 + P_2)^2 = P_1^2 + P_2^2 + 2P_1 \cdot P_2 \approx 2P_1 \cdot P_2$, if we neglect the proton mass, $P_1^2 = P_2^2 = m_p^2$.

Exercise 3.2 – Inserting Eq. (41) into the second term in the Yukawa Lagrangian, Eq. (9), yields

$$\mathcal{L}_Y = -\Gamma_d^{ij} \frac{1}{\sqrt{2}} (v + h) \bar{d}_L^i d_R^j + h.c. \quad (75)$$

(analogous results are obtained for the other terms in the Lagrangian). Using Eq. (13), this can be written

$$\mathcal{L}_Y = -M_d^{ij} \left(1 + \frac{h}{v} \right) \bar{d}_L^i d_R^j + h.c. \quad (76)$$

The field redefinitions that diagonalize the mass matrix, Eq. (15), will therefore also diagonalize the couplings of the fermions to the Higgs boson. The coupling to a given fermion is thus given by $-m_f/v$ (times a factor i since the Feynman rules come from $i\mathcal{L}$), as shown in Fig. 9.

Exercise 3.3 – The answer is evidently no, since these terms connect fields of different chirality.

Exercise 3.4 – In the ultrarelativistic limit, $E \gg m$, the mass of the top quark is negligible. Since helicity is conserved for massless quarks, the top quark and antiquark must be produced with opposite helicities.

Exercise 3.5 – In the limit $E \gg m$ ($\beta \rightarrow 1$), Eq. (48) implies $\psi = \theta$, which means that the off-diagonal and helicity bases are the same. This is as expected, because in the massless limit the helicities of the top quark and antiquark are 100% correlated (see Exercise 3.4), which is the defining characteristic of the off-diagonal basis.

Exercise 3.6 – At threshold ($\beta \rightarrow 0$), Eq. (48) implies $\psi = 0$, which means that the top quark and antiquark spins are 100% correlated along the beam direction. This is a consequence of angular-momentum conservation. At threshold, the top quark and antiquark are produced at rest with no orbital angular momentum. The colliding light quark and antiquark have no orbital angular momentum along the beam direction. Thus spin angular momentum along the beam direction must be conserved. The light quark and antiquark have opposite helicity (due to helicity conservation in the massless limit), so the top quark and antiquark are produced with their spins pointing in the same direction along the beam.

Section 4

Exercise 4.1 – This follows from the unitarity of the CKM matrix, $VV^\dagger = 1$. Displaying indices, this may be written

$$V_{ik}V_{kj}^\dagger = V_{ik}V_{jk}^* = \delta_{ij} . \quad (77)$$

For $i = j$, this implies

$$\sum_{k=d,s,b} |V_{ik}|^2 = 1 , \quad (78)$$

which yields the desired result for $i = t$.

Exercise 4.2 – The square of the four-momentum of the quark propagator in Fig. 21 is

$$p^2 = (k - p')^2 = -2k \cdot p' \quad (79)$$

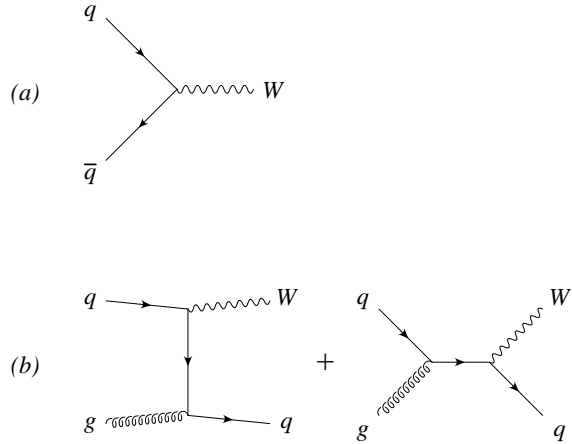


Figure 27. (a) Leading-order subprocess for W production. (b) Leading order subprocess for $W + 1$ jet production.

This vanishes for collinear kinematics,

$$\begin{aligned} k &= (E, 0, 0, E) \\ p' &= (E', 0, 0, E') . \end{aligned}$$

Thus the denominator of the quark propagator vanishes in the collinear limit (if we neglect the quark mass).

Exercise 4.3 – (a) There is just one diagram, shown in Fig. 27(a). (b) There are two contributing subprocesses, $gq \rightarrow Wq$ and $q\bar{q} \rightarrow Wg$; each consists of two Feynman diagrams, shown in Fig. 27(b) for $gq \rightarrow Wq$. The two diagrams for $q\bar{q} \rightarrow Wg$ may be obtained by radiating a gluon off either fermion line in Fig. 27(a).

Exercise 4.4 – The charged-current weak interaction couples only to left-chiral fields. Thus the fermions in the final state (b, ν) have negative helicity, and the antifermion $(\bar{\ell})$ has positive helicity, due to the relationship between chirality and helicity for massless particles (discussed in Section 3).

Exercise 4.5 – In the top-quark rest frame, $s^2 = (0, \hat{\mathbf{s}})^2 = -1$, since $\hat{\mathbf{s}}$ is a unit vector. Because s^2 is Lorentz invariant, this is true in all reference frames. Similarly, $t \cdot s = 0$, because $t = (m, 0, 0, 0)$ in the top-quark rest frame. Thus

$$t_1^2 = \frac{1}{4}(t + ms)^2 = \frac{1}{4}(m^2 - m^2 + 2mt \cdot s) = 0 , \quad (80)$$

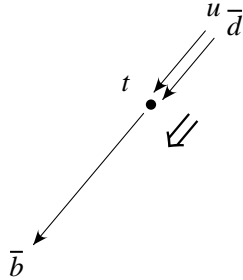


Figure 28. Single-top production in the ultrarelativistic limit, as viewed from the top rest frame.

and similarly for t_2^2 .

Exercise 4.6 – The spatial part of the lightlike four-vector t_2 is pointing in the $-\hat{s}$ direction. Thus $t_2 \cdot \ell \sim 1 - \cos \alpha$, where α is the angle between $-\hat{s}$ and the direction of the charged lepton. This angle is supplementary to θ ($\alpha + \theta = \pi$), so $t_2 \cdot \ell \sim 1 - \cos \alpha = 1 + \cos \theta$.

Exercise 4.7 – The s -channel subprocess, in the top-quark rest frame, looks like Fig. 26. In the limit $E \gg m$, this figure looks like Fig. 28; the u and \bar{d} approach each other along a line and annihilate to make a top quark at rest and a \bar{b} that carries off the incoming momentum. As always, the top-quark spin points in the direction of the \bar{d} . To view this event from the center-of-momentum frame, one boosts opposite the direction of motion of the u and \bar{d} . This boosts the top quark in the direction opposite its spin, so it is in a state of negative helicity. This is as expected; in the limit $E \gg m$, the top quark acts like a massless quark, and is therefore produced in a negative-helicity state by the weak interaction (see Exercise 4.4).

References

- [1] A. F. Falk, “The CKM matrix and the heavy quark expansion,” in *Flavor Physics for the Millennium*, TASI 2000, ed. J. Rosner (World Scientific, Singapore, 2001), p. 379 [arXiv:hep-ph/0007339].
- [2] K. Hagiwara *et al.* [Particle Data Group Collaboration], Phys. Rev. D **66**, 010001 (2002).
- [3] S. Weinberg, “Conceptual Foundations Of The Unified Theory Of Weak And Electromagnetic Interactions,” Rev. Mod. Phys. **52**, 515 (1980) [Science **210**, 1212 (1980)].
- [4] W. Buchmüller and D. Wyler, “Effective Lagrangian Analysis Of New Interactions And Flavor Conservation,” Nucl. Phys. B **268**, 621 (1986).
- [5] R. Bonciani, S. Catani, M. L. Mangano and P. Nason, “NLL resummation of the heavy-quark hadroproduction cross-section,” Nucl. Phys. B **529**, 424 (1998) [arXiv:hep-ph/9801375].
- [6] A. F. Falk and M. E. Peskin, “Production, decay, and polarization of excited heavy hadrons,” Phys. Rev. D **49**, 3320 (1994) [arXiv:hep-ph/9308241].
- [7] M. Peskin and D. Schroeder, *An Introduction to Quantum Field Theory* (Addison-Wesley, Reading, 1995).
- [8] G. Mahlon and S. Parke, “Maximizing spin correlations in top quark pair production at the Tevatron,” Phys. Lett. B **411**, 173 (1997) [arXiv:hep-ph/9706304].
- [9] T. Affolder *et al.* [CDF Collaboration], “First measurement of the ratio $B(t \rightarrow Wb)/B(t \rightarrow Wq)$ and associated limit on the CKM element $|V_{tb}|$,” Phys. Rev. Lett. **86**, 3233 (2001) [arXiv:hep-ex/0012029].
- [10] T. Stelzer, Z. Sullivan and S. Willenbrock, “Single top quark production at hadron colliders,” Phys. Rev. D **58**, 094021 (1998) [arXiv:hep-ph/9807340].
- [11] M. C. Smith and S. Willenbrock, “QCD and Yukawa Corrections to Single-Top-Quark Production via $q\bar{q} \rightarrow t\bar{b}$,” Phys. Rev. D **54**, 6696 (1996) [arXiv:hep-ph/9604223].
- [12] T. Stelzer, Z. Sullivan and S. Willenbrock, “Single-top-quark production via W -gluon fusion at next-to-leading order,” Phys. Rev. D **56**, 5919 (1997) [arXiv:hep-ph/9705398].
- [13] S. Zhu, “Next-To-Leading Order QCD Corrections to $bg \rightarrow tW^-$ at the CERN Large Hadron Collider,” Phys. Lett. B **524**, 283 (2002) [Erratum-ibid. B **537**, 351 (2002)].
- [14] S. S. Willenbrock and D. A. Dicus, “Production Of Heavy Quarks From W -Gluon Fusion,” Phys. Rev. D **34**, 155 (1986).
- [15] M. A. Aivazis, J. C. Collins, F. I. Olness and W. K. Tung, “Leptoproduction of heavy quarks. 2. A Unified QCD formulation of charged and neutral current processes from fixed target to collider energies,” Phys. Rev. D **50**, 3102 (1994) [arXiv:hep-ph/9312319].
- [16] M. Ježabek and J. H. Kühn, “Lepton Spectra From Heavy Quark Decay,” Nucl. Phys. B **320**, 20 (1989).
- [17] G. Mahlon and S. Parke, “Improved spin basis for angular correlation studies in single top quark production at the Tevatron,” Phys. Rev. D **55**, 7249 (1997) [arXiv:hep-ph/9611367].